Accepted Manuscript

Thermochemistry of the E-ALD process for the growth of Cu_xZn_yS on Ag(111): Interpretation of experimental data

Andrea Giaccherini, Giordano Montegrossi, Francesco Di Benedetto, Massimo Innocenti

PII: S0013-4686(17)32745-7

DOI: 10.1016/j.electacta.2017.12.171

Reference: EA 30959

To appear in: *Electrochimica Acta*

Received Date: 16 October 2017

Revised Date: 19 December 2017

Accepted Date: 27 December 2017

Please cite this article as: A. Giaccherini, G. Montegrossi, F. Di Benedetto, M. Innocenti, Thermochemistry of the E-ALD process for the growth of Cu_xZn_yS on Ag(111): Interpretation of experimental data, *Electrochimica Acta* (2018), doi: 10.1016/j.electacta.2017.12.171.

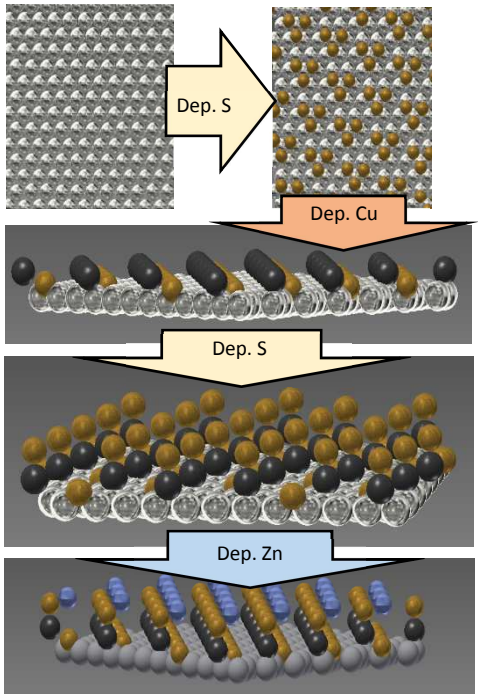
Dep. S
Dep. Cu
Dep. S
Dep. Zn

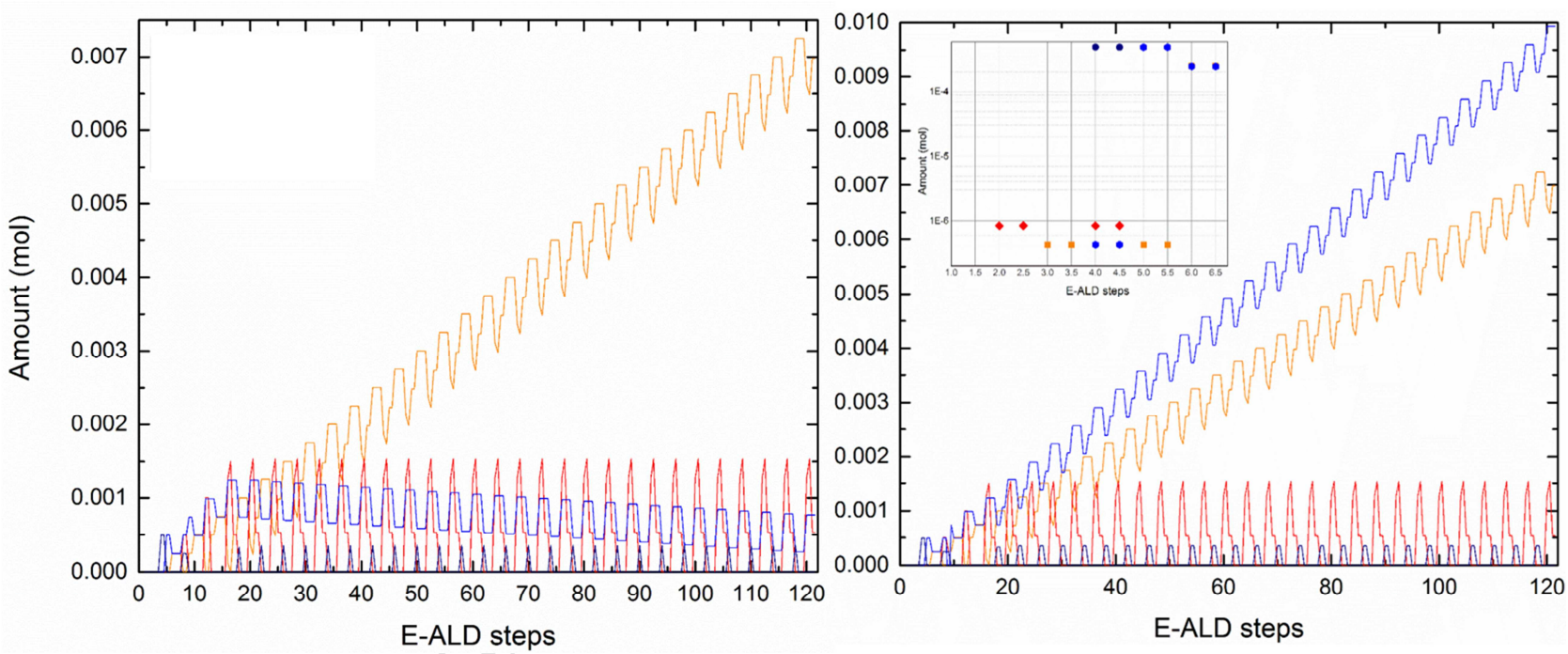
Amount (mol)
E-ALD steps
Amount (mol)
E-ALD steps

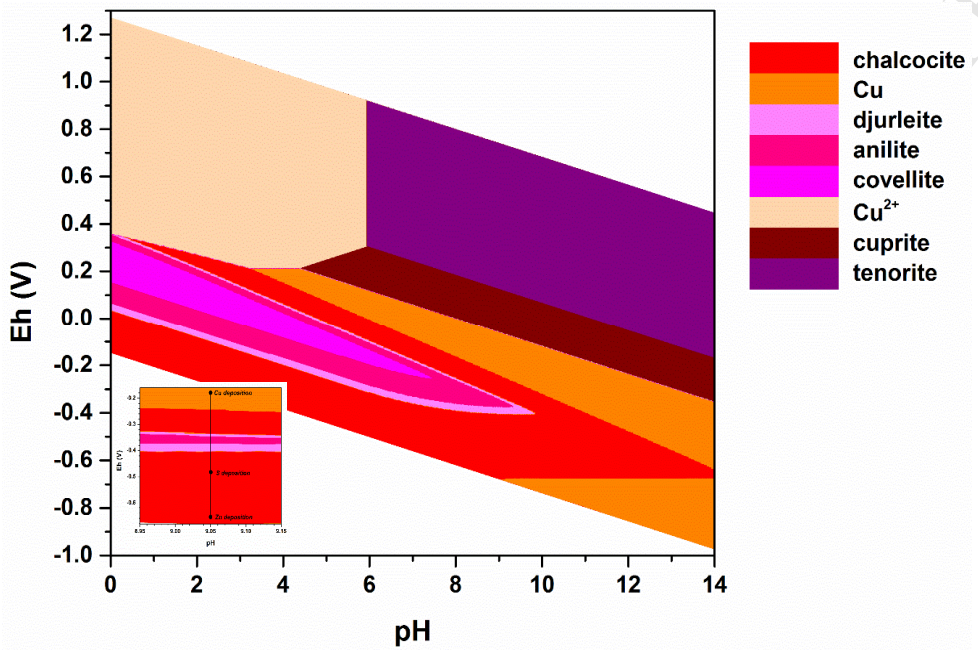
Eh (V)
pH
chalcocite
Cu
djurleite
anilite
covellite
Cu2+
cuprite
tenorite

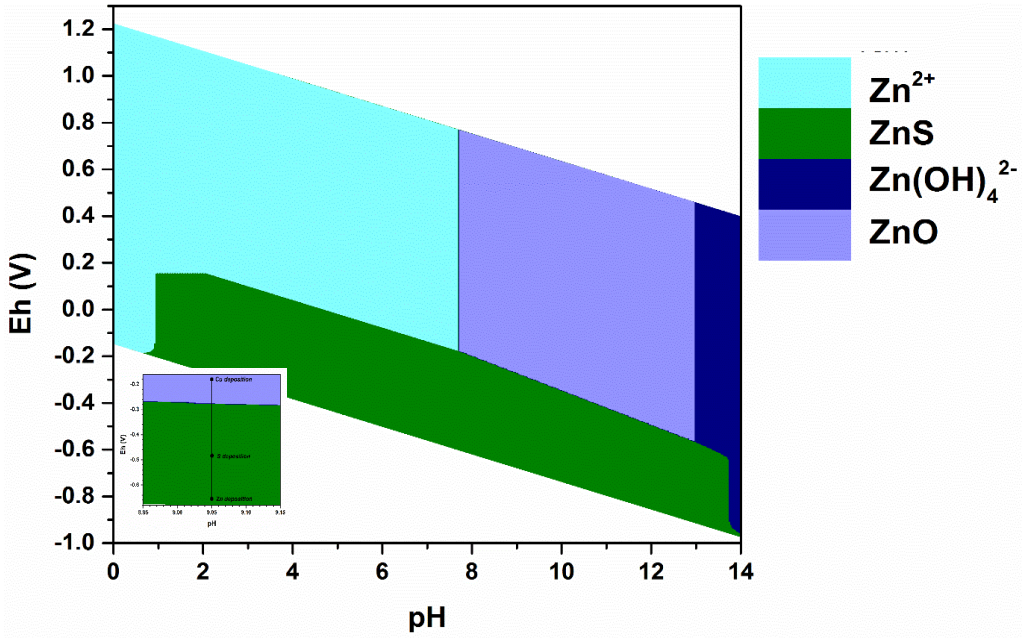
Eh (V)
pH
Zn2+
ZnS
Zn(OH)4 2-
ZnO

Thermochemistry of the E-ALD process for the growth of Cu_xZn_yS on Ag(111): interpretation of experimental data

Andrea Giaccherini[*,1], Giordano Montegrossi[2], Francesco Di Benedetto[2,3] and Massimo Innocenti[1]

* Corresponding author: andrea.giaccherini@unifi.it

[1] Department of Chemistry, Università Degli Studi di Firenze, Via della Lastruccia 3-13, 50019, Sesto Fiorentino (FI), Italy.

[2] IGG-CNR, via G. La Pira 4, 50121, Italy.

[3] Department of Earth Sciences, Università Degli Studi di Firenze, Via La Pira 4, 50121 Firenze, Italy.

Abstract

The electrochemical atomic layer deposition (E-ALD) growth of chalcogenides materials enables the deposition of technologically interesting ultra-thin films. However, this method raises some questions about the actual growth mechanism. We addressed one of the more interesting anomalies reported lately: the occurrence of the Zn-deficiency and of the polycrystalline thread-like overgrown structures in the E-ALD growth of Cu_xZn_yS. The present study was developed using a computational speciation approach under the mass balance method. Exploiting a well-established computational approach, but uncommonly applied to the electrochemical science, we calculated the predominance charts and the equilibrium speciation of the solid phases during the electrochemical process. On this basis, we obtained a deep insight into the mechanism underlying the E-ALD process from a thermodynamic standpoint. Thus, we identified the crucial steps of the Cu_xZn_yS growth leading to the anomalies object of this research.

1. Introduction

The electrochemical atomic layer deposition (E-ALD) exploits surface limited reactions (SLR), such as the underpotential deposition (UPD), to deposit alternate atomic layers of different elements (Figure 1). Being performed at room temperature and pressure, this approach results very effective for the epitaxial growth of metal chalcogenides[1] and more efficient compared to vacuum-based techniques[2]. On this basis, early E-ALD studies have been focussed on the growth of compound semiconductors based on the II-VI elements (e.g CdS, CdSe, CdTe and ZnS) [3–5]. In some cases, the early stages of the E-ALD growth have been studied in great details, by means of *operando* STM (Scanning Tunnel Microscopy) and SXRD (Surface X-Ray Diffraction) experiments[6–9]. Recent developments in the field of thin and ultra-thin films showed an increasing interest for the growth of Earth abundant semiconducting sulfides (including elements as Fe, Zn Sn and Cu)[10–12]. The E-ALD technique was thus successfully used to grow these materials in the form of films several nanometers thick [10,13–15]. These studies found E-ALD to be strongly surface-related, usually considering the oriented

interaction with the surface as the only relevant driving force. In this context, the E-ALD steps are implicitly assumed as independent one to the others. Still, in some cases, different authors found compositional, structural or morphological features conflicting with these assumptions, in particular when growing metal chalcogenides ultra-thin films of *practical thickness*:

a) Unexpected film thickness: 30 E-ALD cycles of CdS are reported to have half the expected thickness [8]

b) Unexpected surface morphology: micrometric scale thread-like structure for the growth of ternary sulfide of copper and zinc (Cu_xZn_yS) [14,16–18].

c) Unexpected chemical composition: the E-ALD growth of copper sulfide results in a Cu:S ratio of 2:1 (Cu_2S) instead of 1:1 (CuS)[19,20]. Similarly, for the growth of Cu_xZn_yS, the expected Cu:Zn ratio was 1:1 while the experimental ratio is 6:1 [14,16–18]. A Zn-deficiency is also found for the growth of Cd_xZn_yS [21].

The fact that the growth process appears, in some way, modulated by additional/external factors pointed out the necessity of further research to better understand the complex nature of the E-ALD.

We present a discussion of the possible causes for the unexpected composition and morphology of Cu_xZn_yS, on the basis of thermodynamics and chemical speciation considerations, taking into account also bulk phases, which are clearly revealed by the presence of these thread-like structure. The idea beyond this approach is that from a sulphide solution at different stages we have different assemblage of deposited sulfides. Thus, the solid phases in equilibrium with the solution can change according to the composition of the solution and to the imposed potentials in agreement with the E-ALD steps. The discussion is based on the chemical speciation at the equilibrium, computed according to the mass balance method. After the introduction, we present a general review of the Cu-Zn-S system, including natural and synthetic phases, in order to set the ground for the modelling process. The third paragraph discusses the modelling methodology applied to this study with a presentation and justification of the assumptions taken on the basis of the known literature. We firstly report the validation of our method for the Zn-O-H by means of comparison with Pourbaix diagrams published by other authors[22] (Cu-S-O-H and Cu-O-H have been elsewhere validated by our group[23]). Then, a general overview of the system is presented through the discussion of the element-specific predominance charts obtained for a multiphasic equilibrium, where the fluid composition takes in to account the salts added for the Cu-Zn-S deposition, the ammonia buffer, (pH=9.13) and the solid precipitating from the solution or already formed in the previous steps. This approach highlights the effect of the concentration and clarifies the relative stability of the solid phases. Finally, we present our speciation model of the step-by-step E-ALD process for the Cu_xZn_yS growth based on the point-by-point mass balance calculation. Although it is a well-established computational procedure in the field of geochemistry, it is worth to notice that it has not been ever applied to the electrochemical science. In the last two sections we present our discussion of the results and the conclusion we can draw about the causes for the unexpected composition and

morphology of Cu_xZn_yS. Every potential reported in this paper is referred to the Standard Hydrogen Electrode (SHE) if not otherwise specified.

2. Phases occurring in the Cu-Zn-S compositional field

The study of the ternary Cu-Zn-S compositional field last from Craig and Kullerud (1973)[24], when they pointed out that small ranges of solid solution occur in the ternary system, especially in the Cu-rich side (thus, Zn-bearing Cu phases are more stable than Cu-bearing Zn phases). However, the extension of these regions is reducing when decreasing the temperature, until they completely disappear at room temperature. Under this condition, therefore, only binary phases are stable. Still, in natural assemblages the co-presence of both Cu- and Zn- binary sulphides is relatively frequent (e.g. hydrothermal ores)[24], whereas the only description of a possible ternary phase, Cu_3ZnS_4, was originally reported by Clark and Sillitoe (1970)[25] and successively mentioned by Fleet (2006)[26]. It is noteworthy to mention that Craig and Kullerud (1973)[24] concluded their study by assessing that no ternary phases were supposed to be stable at room temperature, whereas some minor contents of Cu in Zn sulphides, or of Zn in Cu sulphides has to be considered as metastable phases. Those are considered as the remnant of phases stable at higher temperature or the intermediate product of a replacement process. These considerations confirm the claim that the two cations are supposed to have scarce, or even null, structural and valence affinity when in sulfide systems (without the presence of other chemical species).

Concerning the binary compounds, in nature Cu sulphide minerals are numerous (chalcocite, Cu_2S; djurleite, $Cu_{1.94}S$; digenite, $Cu_{1.8}S$; anilite, $Cu_{1.75}S$; covellite CuS) whereas Zn forms only polymorph minerals with the 1:1 cation-anion ratio (sphalerite, wurtzite and matraite). It is worth to notice that the solubility of Cu in sphalerite seems to be controlled by the presence of trivalent cations (e.g. In, to form roquesite $CuInS_2$ domains, or Fe, to form chalcopyrite $CuFeS_2$ domains) and it is limited to less than 1% by weight at 800 °C [23]. In fact, this fundamental lack of solubility is the origin of the so-called ‘‘chalcopyrite disease’’, which remove all the Cu excess with respect to the allowed solubility in ZnS when associated with chalcopyrite[25]. The redox properties of Cu in sulfides (i.e. the instability of its divalent state in that environment) seems to play a critical role in limiting the stability of Cu–Zn–S structures in thermodynamically equilibrated phases.

Stability lacks for the ternary Cu-Zn-S phases can be, in principle, overcome exploiting kinetic process and out-of-equilibrium conditions. As far as we know, there are few attempts to synthesize mixed Cu-Zn sulphide compounds [27–34]. Uhuegbu et al. claimed to have synthesized Cu-Zn–S compounds through a one-pot synthesis with metal chlorides and thiourea in solution, assisted by opportune complexing agents[27]. Conversely, Aduloju et al. doped ZnS from a contact solution of Cu^{2+}, the resulting products being homogenized by a mild temperature treatment (300 °C)[28]. In a similar way, Kitagawa et al. claimed to have successfully deposited thin films of $Cu_2Zn_2S_3$ by spray pyrolysis[29]. Bagdare et al. presented results about a

nanocrystalline thin film of Cu_xZn_yS obtained by means of chemical bath deposition[30]. Eventually, Adelifard et al. pointed out a byphasic CuS–ZnS thin film by means of spray pyrolysis[31]. Ye et al. suggest the formation of Cu(I)-doped ZnS (ZnS:Cu(I)) nanocrystals under suitable solvothermal conditions with opportune solvent-complexants[32]. Sreejit et al. studied the optical proprieties of the CuZnS deposited by means of chemical spray pyrolysis[33]. Finally, Short et al. report the effective formation of CuS/ZnS multilayer growth by means ALD[34]. Unfortunately, most of these studies lack of a characterisation wide enough to provide conclusively proofs on the presence of accessory phases in the product. This fact can be attributed in part to the fine scale of the exsolution pattern between Cu- and Zn- sulphides, which can prevent its detection unless high magnification techniques, as e.g. the transmission electron microscopy, are taken into account.

3. Computational methods

3.1 Modelling of the equilibria in aqueous solutions

In the present study, the relationships between the main phases of the compositional field (involving always an aqueous solution) are studied through the use of Eh versus pH (or "*Pourbaix*") diagrams, calculated according to the point-by-point mass balance method [23,35]. Under this approach, the predominant charts are computed identifying the predominant species at each given point of potential and pH, taking into account other variables such as presence of ligand(s), temperature and pressure[35]. The predominant species is defined as the one with the highest content (absolute amount) of the considered element, without any discrimination between aqueous and solid species.

We performed our point-by-point mass balance calculation under the *phreeqc* formalism[36]. Aqueous species equilibria are taken into account in a reference database file that include also aqueous complex formation. The solid phases are considered in the same database through dissolution/precipitation reactions, and their stability is reported as the logarithm of equilibrium constant of formation (log K) at standard temperature and pressure condition (i.e. 25°C and 1.0132 bar) from the master species [37,38].

The considered gas species, i.e. $H_{2(g)}$ and $O_{2(g)}$, are computed defining the corresponding partial pressure.In the database are present the dissolution reactions (e.g. $O_{2(g)} = O_{2(aq)}$) and the corresponding constants. Accordingly, the presence of oxygen or hydrogen in any redox reaction is linked to their partial pressure. The latter can be the result of an evolving chemical system or used to constrain the redox potential. The distribution of dissolved components among free ions, ion pairs, and complexes, namely the aqueous speciation, is obtained by solving simultaneously all the equilibria selected from the database. For example, dissolved Cu in the aqueous environment can be present as $Cu^{2+}_{(aq)}$, $Cu^{+}_{(aq)}$, $Cu(OH)_2$, etc.. Among them, $Cu^{2+}_{(aq)}$ act as master species, while the others are defined as secondary species by means of formation reactions from the master species (e.g. $Cu^{2+} + 2OH^- = Cu(OH)_2$, $Cu^{2+} + e^- = Cu^+$, etc.) and their equilibrium

constants (as a function of temperature) are included in the calculations. These species are present in a single phase, an aqueous solution modelled according to the Pitzer acivity model (e.g. Davis, Pitzer or Debye-Huckel activity model)[36].

The model proceeds writing down all the involved reaction for aqueous and gas species and solid phases starting from the master species of the involved elements (Cu, Zn, Sn, C, O and H) and contains all the involved reactions. The system is solved, obtaining the concentrations that satisfy the simultaneous solutions to all the considered equilibria. Numerical models for the chemical speciation requires comprehensive thermodynamic databases.

For this purpose, we referred to the *phreeqc* wateq4f.dat database[39], where the thermodynamic properties of the chemical species relevant to our model were already present . Considering the literature cited in the previous paragraph, we chose to not include any Cu-Zn-S ternary compound or Cu_xS-ZnS solid solution to the wateq4f.dat since none of them is generally accepted as a thermodynamically stable phase at room temperature[24].

3.2 Description of the E-ALD cycles

In order to clarify the thermodynamics of the concurrent reactions underlying the E-ALD process, it is useful to stress the definition of its fundamental blocks, which are represented in Figure 1. The deposition of an atomic layer and the subsequent renovation of the buffer solution in the electrochemical cell (for instance the first two rows in Table 1) at room pressure and temperature, define an E-ALD step. The E-ALD cycle consists of a defined sequence of steps and it is the repetition unit of the whole E-ALD process (for instance the first eight rows in Table 1). Table 1 reports the potential and the solution involved in the E-ALD process modeled in this work, while Figure 2 depicts the time span of the same part of the process.

#Cycle	# Step	E-ALD steps	Conc. (mM)	Time (s)	Pot (V)
1	**1**	**Na_2S/ Buffer**	**0.5**	**60**	**-0.48**
		Buffer	**N/D**	**60**	**-0.48**
	2	**CuCl2/ Buffer**	**0.5**	**120**	**-0.18**
		Buffer	**N/D**	**60**	**-0.18**
	3	**Na2S/Buffer**	**0.5**	**60**	**-0.48**
		Buffer	**N/D**	**60**	**-0.48**
	4	**$ZnSO_4$/ Buffer**	**0.5**	**120**	**-0.65**
		Buffer	**N/D**	**60**	**-0.65**
2	5	Na_2S/ Buffer	0.5	60	-0.48
		Buffer	N/D	60	-0.48
	6	$CuCl_2$/ Buffer	0.5	120	-0.18
		Buffer	N/D	60	-0.18

Table 1: The first 8 rows, in bold, constitute the E-ALD cycle.

The deposition of the first Sulfur adsorbed atomic layer (briefly S-adlayer) on the Ag(111) surface requires a deeper analysis regarding the S-adlayer. Since the surface crystallographic cell of the Ag-S interface includes 3 sulfur atoms and 6 silver atoms (Figure 1b), its apparent surface stoichiometry is Ag_2S (the mineral acanthite).-The excess of free energy obtained by (Aloisi et. al [6]), is indeed required to model the deposition step of the S-adlayer, that otherwise would result slightly unstable. Thus, the modelling procedure was carried out as follows:

a) Modelling of the formation of the S-adlayer by precipitation of Ag_2S (acanthite) driven by the additional surface free energy.
b) Modelling of the subsequent steps using the thermodynamic data for the bulk phases. As a starting condition of each step, we considered the amount of solid phases obtained at the equilibrium of the previous step in contact with fresh solutions under the proper potential.

It is useful to remark that, between two following E-ALD steps, the solution is changed, while keeping a constant applied potential. In order to assure a complete change of the chemical environment inside the cell, the volume of fluxed solution is several times the volume of the cell (roughly 30 times). Conversely, in the modelling of E-ALD, the solution volumes are kept constant at the value of the cell volume, thus largely underestimating the effect of the dissolution processes during the exchange of solution. We refer to this calculation as *constant volume model*. To overcome this limitation, a further calculation was carried out under the assumption that the moderately soluble phases are completely dissolved while fluxing the washing solution: this model overestimates the effect of the dissolution processes. We referred to this last calculation as *total depletion model*. In this context, it is evident that the *total depletion model* has been defined after having identified the most soluble species in the *constant volume model*.

3.3 Thermodynamic conditions

In order to perform a reliable computational description of the chemical speciation occurring at the interface, the thermodynamic conditions of the process were carefully constrained. In particular, while the potential is finely controlled by means of the three electrodes electrochemical cell, the pH could change due to the degassing of the solutions or to the effect of the potential. We measured the pH of the fresh buffer solution and after degassing, and under operative conditions at the lowest (-1.4V) and highest (0.1V) applied potentials. The measurements have been carried by means of the “827pH Lab” (Metrohm) pH meter,

calibrated with standard buffer solutions, pH=7 and pH=10 (Metrohm). The results are presented in Table 2. Accordingly, the E-ALD process were modelled at pH=9.05.

Fresh buffer	30' degassing	1' at -1.6V	1' at -0.1V
9.12(5)	9.05(5)	9.06(5)	9.04(5)

Table 2: Changes of the pH during the E-ALD

4 Results and discussion

4.1 Predominance charts of the Zn-O-H system

Figure 3 shows the diagram for Zn-O-H system computed taking into account a total zinc molality of 1 10^{-6} mol/kgw ([Zn] =1 10^{-6} mol/kgw), finding an excellent agreement with the literature[22,40]. Comparing Pourbaix diagrams (calculated by the line method)[22,40] with the diagram in Figure 3, (calculated by the mass balance method), indeed, only two different features are present(shown in the inset to Figure 3). There is a very small stability field of the ZnO in the lower part of the diagram (pointed by the arrow). Moreover, the $Zn^{2+}/Zn(OH)_2$ stability boundary is curved. Both these features were not accountable by the line method.

Figure 4a depicts the Pourbaix diagram for the Zn-S system calculated in the following conditions: [Zn]=1 10^{-4} mol/kgw [S] =1 10^{-3} mol/kgw. A small discrepancy in the stability field of ZnS, at high pH values, is observed between the present results and the work presented by Peters[41]. This difference is likely due to the effect of the competitive equilibria with minor species (aqueous complex of Zn with various stoichiometry) that are not taken into account by the precedent paper on this subject. Figure 4b highlights the effect of the concentration, at [Zn]=1 10^{-6} mol/kgw [S]=1 10^{-3} mol/kgw the stability field of the ZnS sphalerite is reduced while $Zn(OH)_2$ becomes predominant over zincite.

4.2 Predominance charts of the Cu-Zn-S-O-H system

This system represents a solution of Zn and Cu salts in ammonia buffer (50mM of NH_3 and 25mM of $HClO_4$) at the equilibrium with the solid phases, hence it constitutes a general description of the chemical environment where the E-ALD growth is performed (shortly the E-ALD environment). Figures 5, 6 and 7 depict the predominance charts specific for each relevant elements in the Cu-Zn-S-O-H system (respectively Cu, S and Zn). In order to clarify the change of the speciation with the concentration of the main species, we present the predominance chart for each of the environments presented in Table 3.

Environment	[Cu] (mol/kgw)	[Zn] (mol/kgw)	[S] (mol/kgw)
a)	5 10^{-4}	5 10^{-4}	5 10^{-3}
b)	1 10^{-5}	1 10^{-5}	1 10^{-3}
c)	1 10^{-6}	1 10^{-6}	1 10^{-3}

Table 3 Formal concentration of the elements in the three environments hereby discussed.

The a) environment is very close to what realized during the E-ALD synthesis, in the sense that the formal concentrations of the chemical species are the same of the metal salts in the solution used for the E-ALD. The main difference with E-ALD environment is the formal concentration of S which is 5 10^{-3} mol/kgw. The excess of sulfur formal concentration with respect to metals is a common practice to compute the predominance charts within the *phreeqc* framework, to prevent sulfur from acting as a limiting species for the precipitation of sulphides[23,42]. Environments b) and c), on the other hand, have been calculated with lower formal concentrations in order to highlight the effect of the concentration on the relative stability of the solid phases and to make them comparable with literature's data on the Cu-S-OH, Cu-O-H, Zn-S-OH and Zn-O-H subsystems. We have also calculated the predominance charts in the system Cu-Zn-S-O-H and compared them to those here presented (Cu-Zn-S-N-Cl-O-H), finding only negligible differences regarding the solvated species (for this reason, the relative Pourbaix diagrams are not shown).

Figure 5 depicts the predominance charts of the copper-bearing species. It is worth noting that chalcocite results as the most stable sulfide phase. In general, the stability fields of sulphides phases do not significantly change within the considered concentration range. Most of the changes related to the concentrations are in the upper part of the diagrams, related to Cu-O species. Figure 5a reports the predominance chart for copper-bearing species in the E-ALD environment. As elsewhere reported for other environments[23], in the lower part of the plots (more reducing conditions) copper sulphides phases dominate the charts. In the upper part of the plots copper oxides are the most abundant phases. The only region where solid phases are lacking occurs at very low pH under anodic conditions, where Cu^{2+} is the main aqueous species. The inset in Figure 5a roughly depicts the range of pH and potential where the whole E-ALD occurs, giving an insight about the most stable solid phases involved in the growth of Cu_xZn_yS: these species result elemental copper and chalcocite. Figure 5b shows the reduction of the stability field of tenorite while lowering the formal concentration of the chemical species. Figure 5c resembles very closely the Pourbaix plots for the Cu-S system elsewhere published [23,41,43].

Figure 6 shows the predominance charts of the sulphur-bearing species. The only clear trend is the reduction of the stability field of elemental sulfur while lowering the formal sulfur concentration. The other stability fields are very similar in the three environments. A comparison of figure 6b,c with the Pourbaix diagrams of the Cu-S system reported by Peters[41] and Huang[42] shows that the only difference is the reduced stability of elemental sulfur. The absence of reduced aqueous sulfur species is evident in the upper part of our diagram. These discrepancies with Cu-S system have to be accounted for the presence of competitive equilibria involving also the precipitation of zinc and copper sulphides as well as other redox equilibria in the liquid phase. Figure 7 depicts the predominance charts for the zinc-bearing species. In particular, figure 7b compared to Figure 4a shows that the stability field of solid phases extends at higher pH in the E-ALD environment with respect to the Zn-S-OH system. Moreover, it should be noticed that the potentials at which we perform the E-ALD steps (inset in figure 7a) is across the ZnO/ZnS stability boundary.

4.3 The E-ALD cycles

According to the results described in the last section, the only solid phases precipitating during the process (except the first step) are chalcocite, sphalerite, Cu and zincite. Here below, the results are discussed according to the constant volume and total depletion models separately including only these species.

Costant volume model

Figure 8 shows the plot of the cumulative molar amount of the main solid phases as a function of the number of E-ALD steps. A transient regime of the chemical speciation for the first 20 steps is apparent. Successively, the system reaches a periodicly increasing regime. Further detail on the transient regime is given in the inset to figure 8, where a close-up on the first 6 steps (Table 1) is shown. In general, the cleaning constituting the last part of each deposition step do not affect the amount of precipitated phases. To improve the readability of the graphs we didn't report the amount of acanthite in the Figures 8 and 10. However, we find that the first step deposits the S-adlayer as expected, due to the excess of free energy added to the acanthite species to model the strong interaction with the Ag(111) surface. Hence none of the 4 relevant solid phases (copper, chalcocite, zincite and sphalerite) are present after the first step. The second step (reduction of copper) results in the precipitation of metallic copper. The third step (deposition of sulfur) lead to the complete sulfidization of the metallic copper, converted completely to chalcocite. The fourth step lead to the deposition of the zinc as zincite and the desulfidization of chalcocite leading to the formation of sphalerite and metallic copper. The fifth step lead to the complete sulfidization of metallic copper and zincite converted respectively in chalcocite and sphalerite. The sixth step of this sequence is the deposition of copper. At this stage, we observe the formation of chalcocite at the expenses of sphalerite, which can be assigned to the higher stability of the former. Although the sixth step leads clearly to a decrease of total Zn in the solid phases, unexpectedly the process monitored over 120 steps (Figure 8) shows steady growth of chalcocite and sphalerite over zincite and metallic copper. Sphalerite appears to be dominant in the solid phases over chalcocite. This is due to the different metal to sulfur ratio in chalcocite (2:1) and sphalerite (1:1). Hence, considering the amounts normalized over the metal atoms per unit formula, we get 0.0146 equivalents of chalcocite against 0.010 of sphalerite.

During the periodic regime (after 20 steps) every time copper is deposited, the total amount of zinc in the solid phase is reduced (Figure 9a), while during the whole process lacks a net decrease of copper in the solid phases (Figure 9b). Moreover, Figure 8 confirms zincite as the less stable solid phase when the reduction of the amount of Zn in the solid phase occurs (during the deposition of copper).

Total depletion model

The total depletion model has been developed under the assumption that during the flux of the copper solution inside the cell (fluxing a volume several times bigger than the cell volume, to change the solution) zincite is completely depleted. The results of such model are depicted in Figure 10, where it is possible to observe that in this case the only species increasing monotonically over the cycles is chalcocite. Conversely, sphalerite slowly decreases after the 20th cycle. Thus, the Cu/Zn ratio at the end of the process is by far larger than the ratio obtained with the constant volume model (18.9). Recalling that Figures 8 and 10 depict the main results of the constant volume and total depletion models, respectively, Table 4 shows the comparison of the expected Cu/Zn ratio with the experimental data after 120 steps[14,16,17].

	Cu/Zn	**REF**
Constant volume	1.46	This study
Total depletion	18.9	This study
Experimental $Cu_{0.83}Zn_{0.17}S$	6	[16]

Table 4 comparison between the theoretical and experimental Cu/Zn ratios.

5. Discussion

The element specific predominance charts have been presented in order to understand the overall stability of solvated and solid species in the Cu-Zn-S-O-H system, the system conventionally adopted to synthesize phases of the Cu-Zn-S system over Ag(111) through E-ALD[16–18]. The Pourbaix diagrams allowed to identify the four main metal-bearing species involved in the E-ALD process: chalcocite, Cu, zincite and sphalerite. The relevance of these 4 species is confirmed also by the calculation of the E-ALD steps, carried by means of the two extremes models:

1) “Constant volume”

2) “Total depletion”

In this context, the pursued computational approach demonstrated that the dominant phase in the bulk of the grown material is chalcocite.

- Regarding the Zn-deficiency: table 4 shows that the experimental Cu/Zn is 6:1, hence between the two value of 18.9:1 (total depletion model) and 1.46:1 (constant volume model). Since the theoretical value don’t match the experiments, we suggest that the depletion of zincite during the reduction of copper is not complete as we assumed for the “total depletion model”. We consider such incomplete depletion as related to the following factors: the contemporary growth of a surface driven epitaxial phase, the kinetics of the dissolution processes and the convective transport of dissolved species during the renewal of the solution. However, we found a net decrease of zinc (between 0.3% and 1% even in the constant volume model), suggesting that the periodic

interconversion of Zn between sulfidized and oxidized species, and the preferential dissolution of zincite, are the cause of the Zn-deficiency in the E-ALD growth of Cu_xZn_yS.

- Regarding the overgrown thread-like structure: both our models forecast a prevalent amount of chalcocite. Since most of the polycrystalline phase in the Cu_xZn_yS samples is chalcocite[16], we suggest that the occurrence of the thread-like structure is related to the precipitation/dissolution equilibria involving the 4 relevant species when depositing copper. In these conditions, the net results is the precipitation of bulk chalcocite at the expense of sphalerite (involving sphalerite to zincite dissolution-precipitation reactions and partial zincite dissolution).

To explain in deeper details the process we propose a mechanism grounded on the following five competing equilibria guessed on the basis of the complete simultaneous equilibria system described in the "Computational methods" section:

$$Cu^{2+} + 2\ e^- \Leftrightarrow Cu_{(s)} \quad (1)$$

$$Zn^{2+} + 2\ OH^- \Leftrightarrow ZnO + H_2O \quad (2)$$

$$2\ Cu_{(s)} + 2\ HS^- \Leftrightarrow Cu_2S_{(s)} + H_2O + 2\ e^- \quad (3)$$

$$ZnO_{(s)} + HS^- \Leftrightarrow ZnS_{(s)} + OH^- \quad (4)$$

$$ZnO_{(s)} + H_2O \Leftrightarrow Zn(OH)_{2(aq)} \quad (5)$$

Equilibria 1-2 are mainly involved during the steps leading to the deposition of Cu and zincite (second and fourth steps, Fig. 2). Equilibria 3-4 are involved in the deposition of sulfur, leading to the sulfidization of Cu and zincite (third and fifth steps, Fig. 2). Starting from the sixth step, everytime that a solution of Cu^{2+} is kept at -0.18 V, the presence of solid sulphides enables the formation of chalcocite at the expense of sphalerite through the competition of equilibria 1-4, resulting also in a partial conversion of sphalerite to zincite. Moreover, equilibrium 5 is responsible for the decrease of the total Zn content in the solid phases (at a rate of 0.3-1 % w/w per cycle) through the dissolution of zincite.

6. Conclusion

The E-ALD growth of chalcogenides materials enables the deposition of technologically interesting ultra-thin films while leading to a series of unexpected results (i.e. Cu_2S, CdS, Cu_xZn_yS and $Cd_xZn_{1-x}S$). These results raise several questions about the actual growth mechanism. In the present paper, we addressed one of the more interesting open question in this field: the occurrence of the Zn-deficiency and of the polycrystalline thread-like overgrown structures in the E-ALD growth of Cu_xZn_yS. The present study was developed using a computational speciation approach, designing models under the mass balance method in the *phreeqc* framework. Our approach was carefully validated through the comparison of our predominance charts with

the literature on the Zn-O-H subsystem. As far as we know, an unprecedented Pourbaix diagram of the Zn-S-O-H system is shown.

Our approach reproduced the trends found in literature[16,18,19], giving a clear (although qualitative) insight in the growth process and allowing to discriminate the possible causes for the Zn-deficiency and the thread-like structure in the Cu_xZn_yS films.

The unprecedented application of speciation models to the E-ALD process was able to confirm the link between the Zn-deficiency, the arising of the thread-like structure and the dissolution of Zn during the Cu deposition step. These structures constitute one of the more interesting results among the completely unexpected results series reported for CdS, Cu_2S, $Cd_xZn_{1-x}S$ and Cu_xZn_yS [7,8,16,17,21].

Finally, as shown by the results found for the S-adlayer deposition, given the access to a good estimation of the excess of free energy at the surface, our computational approach could be easily extended to the epitaxial phases. Given this last observation and considering that the speciation models were applied successfully to other electrochemical studies, it is opinion of the authors that this approach could find general application in the analysis of competitive reactions occurring in electrochemical systems.

Aknowledgements

FDB and MI benefited for departmental funding (ex 60%). CNR is acknowledged, for support.

Bibliography

1. Stickney, B. W. & Gregory, J. L. Electrochemical atomic layer epitaxy (ecale). *J. Electroanal. Chem.* **300,** 543–561
2. Innocenti, M. *et al.* Fabricating energy devices with low environmental impacts. *SPIE Newsroom* 2–4 (2016). doi:10.1117/2.1201512.006249
3. M. Innocenti, G. Pezzatini, F. Forni, and M. L. F. CdS and ZnS Deposition on Ag(111) by Electrochemical Atomic Layer Epitaxy. *J. Electrochem. Soc.* **148,** C357–C362 (2001).
4. Huang, B. M., Colletti, L. P., Gregory, B. W., Anderson, J. L. & Stickney, J. L. Preliminary studies of the use of an automated flow-cell electrodeposition system for the formation of CdTe thin films by electrochemical atomic layer epitaxy. *J. Electrochem. Soc.* **142,** 3007–3016 (1995).
5. Publishing, E., Parashchuk, T. O., Freik, N. D. & Fochuk, P. M. DFT-Calculations of Thermodynamic Parameters of ZnTe, ZnSe, ZnS Crystals. *Phys. Mater. Chem.* **2,** 14–19 (2014).
6. Aloisi, G. D. *et al.* In situ STM and electrochemical investigation of sulfur oxidative underpotential deposition on Ag(111). *J. Phys. Chem. B* **101,** 4774–4780 (1997).
7. Giaccherini, A. *et al.* Operando SXRD study of the structure and growth process of Cu2S ultra-thin

films. *Sci. Rep.* **In-press,** (2017).

8. Carlà, F. *et al.* Electrochemical atomic layer deposition of CdS on Ag single crystals: Effects of substrate orientation on film structure. *J. Phys. Chem. C* **118,** 6132–6139 (2014).

9. Foresti, M. L. *et al.* In situ X-ray analysis under controlled potential conditions: An innovative setup and its application to the investigation of ultrathin films electrodeposited on Ag(1 1 1). *Electrochim. Acta* **51,** 5532–5539 (2006).

10. Valdes, M., Modibedi, M., Mathe, M., Hillie, T. & Vazquez, M. Electrodeposited Cu2ZnSnS4 thin films. *Electrochim. Acta* **128,** 393–399 (2014).

11. Kask, E., Raadik, T., Grossberg, M., Josepson, R. & Krustok, J. Deep defects in Cu2ZnSnS4 monograin solar cells. *Energy Procedia* **10,** 261–265 (2011).

12. Zillner, E. *et al.* Lattice positions of Sn in Cu2ZnSnS4 nanoparticles and thin films studied by synchrotron X-ray absorption near edge structure analysis. *Appl. Phys. Lett.* **102,** 2–6 (2013).

13. Caporali, S. *et al.* Sn-deficiency in the electrodeposited ternary CuxSnySz thin films by ECALE. *Sol. Energy Mater. Sol. Cells* **138,** 9–16 (2015).

14. Innocenti, M. *et al.* Electrochemical growth of Cu-Zn sulfides. *J. Electroanal. Chem.* **710,** 17–21 (2013).

15. Innocenti, M. *et al.* Electrochemical layer by layer growth and characterization of copper sulfur thin films on Ag(1 1 1). *Electrochim. Acta* **58,** 599–605 (2011).

16. Innocenti, M. *et al.* Electrochemical Growth of Cu-Zn Sulfides of Various Stoichiometries. *ECS Trans.* **161,** D14–D17 (2014).

17. Di, F. *et al.* Electrodeposited semiconductors at room temperature : an X-ray Absorption Spectroscopy study of Cu- , Zn- , S-bearing thin fi lms. *Electrochim. Acta* **179,** 495–503 (2015).

18. Di Benedetto, F. *et al.* Physical Characterization Of Thin Films Of CuxZnySz For Photovoltaic Applications. *ECS Trans.* **58,** 59–65 (2013).

19. Giaccherini, A., Felici, R. & Innocenti, M. in *X-ray Characterization of Nanostructured Energy Materials by Synchrotron Radiation* In press (In-tech, 2017).

20. Giaccherini, a. *et al.* Synthesis and Technological Application of Electrodeposited Semiconductors by EC-ALD. *ECS Trans.* **58,** 35–41 (2014).

21. Innocenti, M. *et al.* Ternary cadmium and zinc sulfides: Composition, morphology and photoelectrochemistry. *Electrochim. Acta* **49,** 1327–1337 (2004).

22. Beverskog, B. & Puigdomenech, I. Revised pourbaix diagrams for zinc at 25–300 {{\textdegree}C}. *Corros Sci* **39,** 107–114 (1997).

23. Giaccherini, A., Montegrossi, G. & Di Benedetto, F. Stability of Naturally Relevant Ternary Phases in the Cu–Sn–S system in Contact with an Aqueous Solution. *Minerals* **6,** 79 (2016).

24. Craig, J. R. & Kullerud, G. The Cu-Zn-S system. *Miner. Depos.* **8,** 81–91 (1973).

25. Clark, A. H. & Stillitoe, R. H. Cuprian sphalerite and probable copper-zinc sulfide and probable copper-zinc sulfide. *Am. Mineral.* **55,** 1021–1025 (1970).

26. Fleet, M. E. Phase Equilibria at High Temperatures. *Rev. Mineral. Geochemistry* **61,** 365–419 (2006).

27. Uhuegbu, C. C. & Babatunde, E. B. The Study of Copper Zinc Sulphide (CuZnS 2) Thin Films. *J. Phys. (main title)* **32,** 39–47 (2008).

28. K.A. Aduloju, A. I. M. Optical absorption and transmission in CuZnS alloys. *Glob. J. Pure Appl. Sci.* **15,** 421–425 (2009).

29. Kitagawa, N. Copper Zinc Sulfur Compound Solar Cells Fabricated by Spray Pyrolysis Deposition for Solar Cells. *Nat. Resour.* **4,** 142–145 (2013).

30. Bagdare, P. B., Patil, S. B. & Singh, A. K. Phase evolution and PEC performance of ZnxCd(1-x)S nanocrystalline thin films deposited by CBD. *J. Alloys Compd.* **506,** 120–124 (2010).

31. Adelifard, M., Eshghi, H. & Bagheri Mohagheghi, M. M. Synthesis and characterization of nanostructural CuS-ZnS binary compound thin films prepared by spray pyrolysis. *Opt. Commun.* **285,** 4400–4404 (2012).

32. Ye, H. *et al.* Facile one-step synthesis and transformation of Cu(I)-doped zinc sulfide nanocrystals to Cu1.94S-ZnS heterostructured nanocrystals. *Langmuir* **29,** 8728–8735 (2013).

33. Sreejith, M. S., Deepu, D. R., Kartha, C. S. & Vijayakumar, K. P. Tuning of properties of sprayed CuZnS films. *AIP Conf. Proc.* **1591,** 1741–1743 (2014).

34. Short, A. *et al.* Structure in multilayer films of zinc sulfide and copper sulfide via atomic layer deposition. *J. Vac. Sci. Technol. A Vacuum, Surfaces, Film.* **32,** 01A125 (2014).

35. Huang, H. The Eh-pH Diagram and Its Advances. (2016). doi:10.3390/met6010023

36. Parkhurst, B. D. L. & Appelo, C. a J. User's Guide To PHREEQC (version 2) — a Computer Program for Speciation, and Inverse Geochemical Calculations. *Exch. Organ. Behav. Teach. J.* **D,** 326 (1999).

37. Helgeson, H. C., Delany, J. M., Nesbitt, H. W. & Bird, D. K. Summary and Critique of the Thermodynamic Properties of Rock-Forming Minerals. *Am J Sci* **278–A,** (1978).

38. Johnson, J. W., Oelkers, E. H. & Helgeson, H. C. *SUPCRT92: A software package for calculating the standard molal thermodynamic properties of minerals, gases, aqueous species, and reactions from 1 to 5000 bar and 0 to 1000??C. Computers and Geosciences* **18,** (1992).

39. Ball, J. W. & Nordstrom, D. K. User's Manual for WATEQ4F, with revised thermodynamic data base and test cases for calculating speciation of major, trace, and redox elements in natural waters. *U.S. Geol. Surv. Water-Resources Investig. Rep.* **91–183,** 1–188 (1991).

40. Popov, B. N. *Corrosion Engineering: Principles and Solved Problems*. *Corrosion Engineering: Principles and Solved Problems* (2015). doi:0444627227

41. Peters, E. The 1976 Extractive Metallurgy Lecture The Metallurgical Society of AIME Direct Leaching of Sulfides : Chemistry and Applications. (1976).

42. Huang, H.-H. The Eh-pH Diagram and Its Advances. *Metals (Basel).* **6,** 23 (2016).

43. Young, C. A., Dahlgren, E. J. & Robins, R. G. The solubility of copper sulfides under reducing conditions. *Hydrometallurgy* **68,** 23–31 (2003).

Captions to figures

Figure 1 Pictorial representation of the main mechanism for the first stages of the E-ALD growth of the Cu_xZn_yS: a) the Ag(111) surface, b) the sulfur (dark yellow) atoms on the Ag(111), the black parallelogram showing the repetition motive, c) the deposition of the copper atoms (black), d) the growth of the second sulfur layer and e) the deposition of the zinc atomic layers (blue).

Figure 2 Time span of the E-ALD cycle considered in this work. The blue and brown arrows highlight the E-ALD steps and cycles, respectively. S represents the presence inside the electrochemical cell of the Na_2S solution, B the buffer, Cu the $CuCl_2$ and Zn the $ZnSO_4$ solutions, respectively.

Figure 3 Pourbaix diagram for the Zn-O-H system; the inset shows two features that can only be accounted by means of the point-by-point method ([Zn]=1 10^{-6} mol/kgw).

Figure 4 Pourbaix diagrams of the Zn-S-O-H system assuming a) [Zn]=1 10^{-4} mol/kgw [S]=1 10^{-3} mol/kgw b) [Zn]=1 10^{-6} mol/kgw [S]=1 10^{-3} mol/kgw.

Figure 5 Predominance charts for the Copper bearing phases, assuming a) [Zn]=5 10^{-4} mol/kgw [Cu]=5 10^{-4} mol/kgw [S]=5 10^{-3} mol/kgw b) [Zn]=1 10^{-5} mol/kgw [Cu]=1 10^{-5} mol/kgw [S]=1 10^{-3} mol/kgw c) [Zn]=1 10^{-6} mol/kgw [Cu]=1 10^{-6} mol/kgw [S]=1 10^{-3} mol/kgw.

Figure 6 Predominance charts for the sulfur bearing phases, assuming a) [Zn]=5 10^{-4} mol/kgw [Cu]=5 10^{-4} mol/kgw [S]=5 10^{-3} mol/kgw b) [Zn]=1 10^{-5} mol/kgw [Cu]=1 10^{-5} mol/kgw [S]=1 10^{-3} mol/kgw c) [Zn]=1 10^{-6} mol/kgw [Cu]=1 10^{-6} mol/kgw [S]=1 10^{-3} mol/kgw.

Figure 7 Predominance charts for the Zinc bearing phases, assuming a) [Zn]=5 10^{-4} mol/kgw [Cu]=5 10^{-4} mol/kgw [S]=5 10^{-3} mol/kgw b) [Zn]=1 10^{-5} mol/kgw [Cu]=1 10^{-5} mol/kgw [S]=1 10^{-3} mol/kgw c) [Zn]=1 10^{-6} mol/kgw [Cu]=1 10^{-6} mol/kgw [S]=1 10^{-3} mol/kgw.

Figure 8 Amount of the solid species as computed by means of the constant volume model. In the inset and the main plot the blue, red, yellow and blue curves represents the total amounts of Sphalerite, Chalcocite, Copper and Zincite respectively.

Figure 9 Amount of the total metal ions in the liquid phase compared to the change of the amount of solid phases (constant volume model).

Figure 10 Amount of the solid species as computed by means of the total depletion model. In the plot the blue, red, yellow and blue curves represents the total amounts of Sphalerite, Chalcocite, Copper and Zincite respectively.

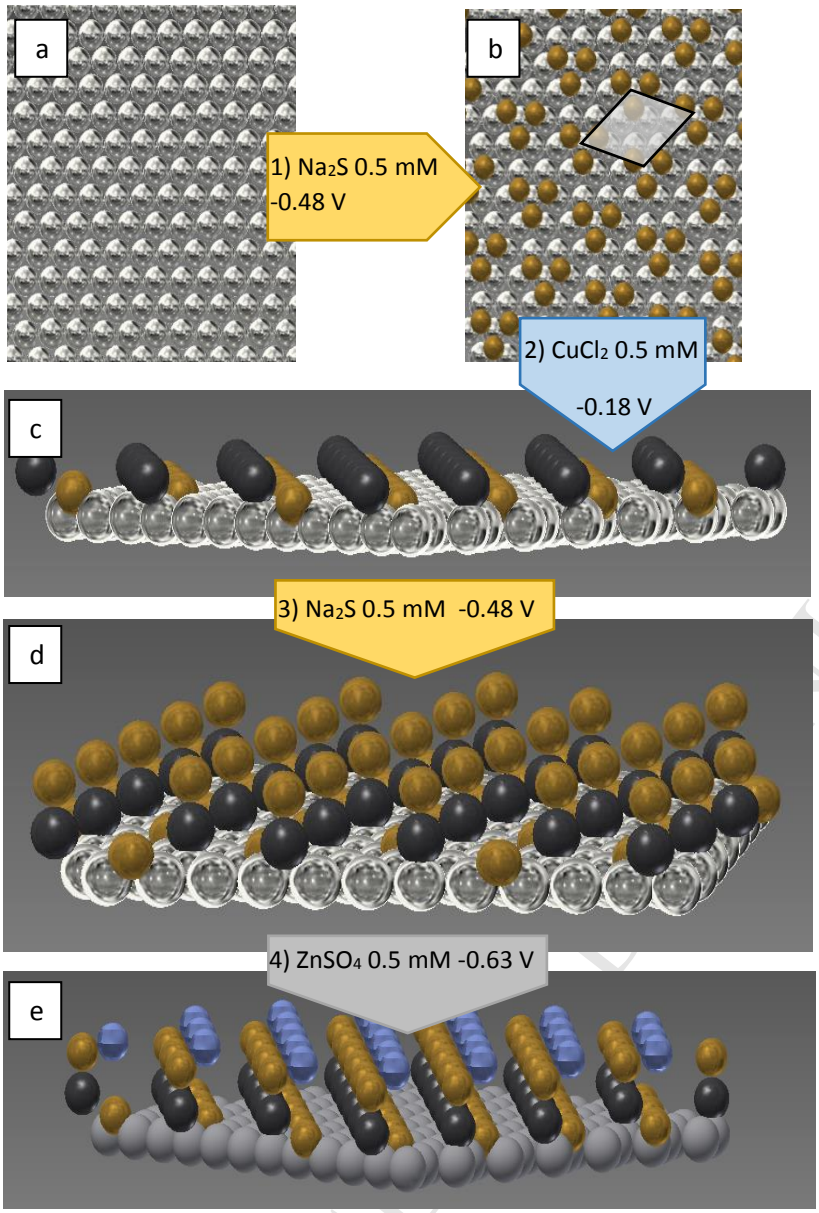

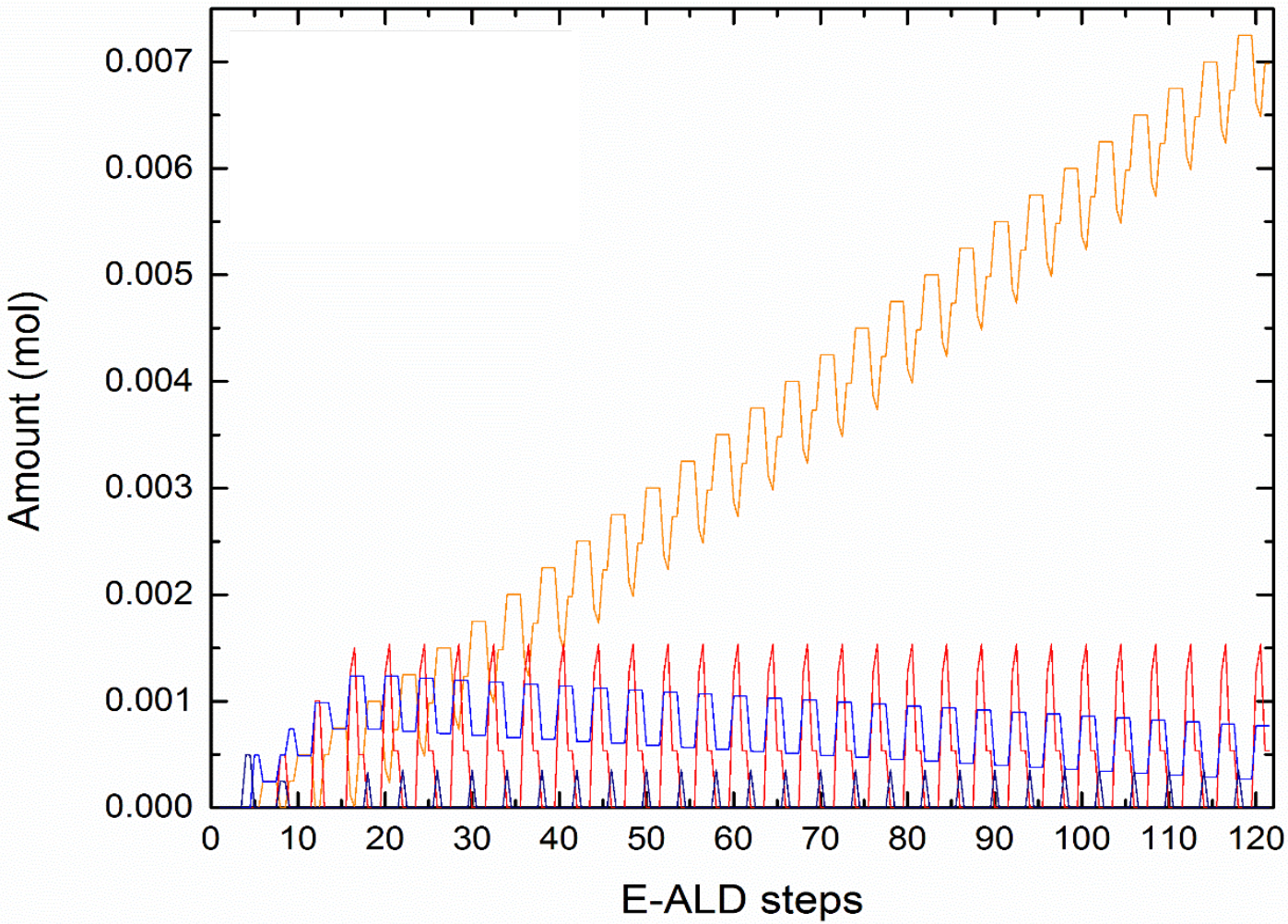

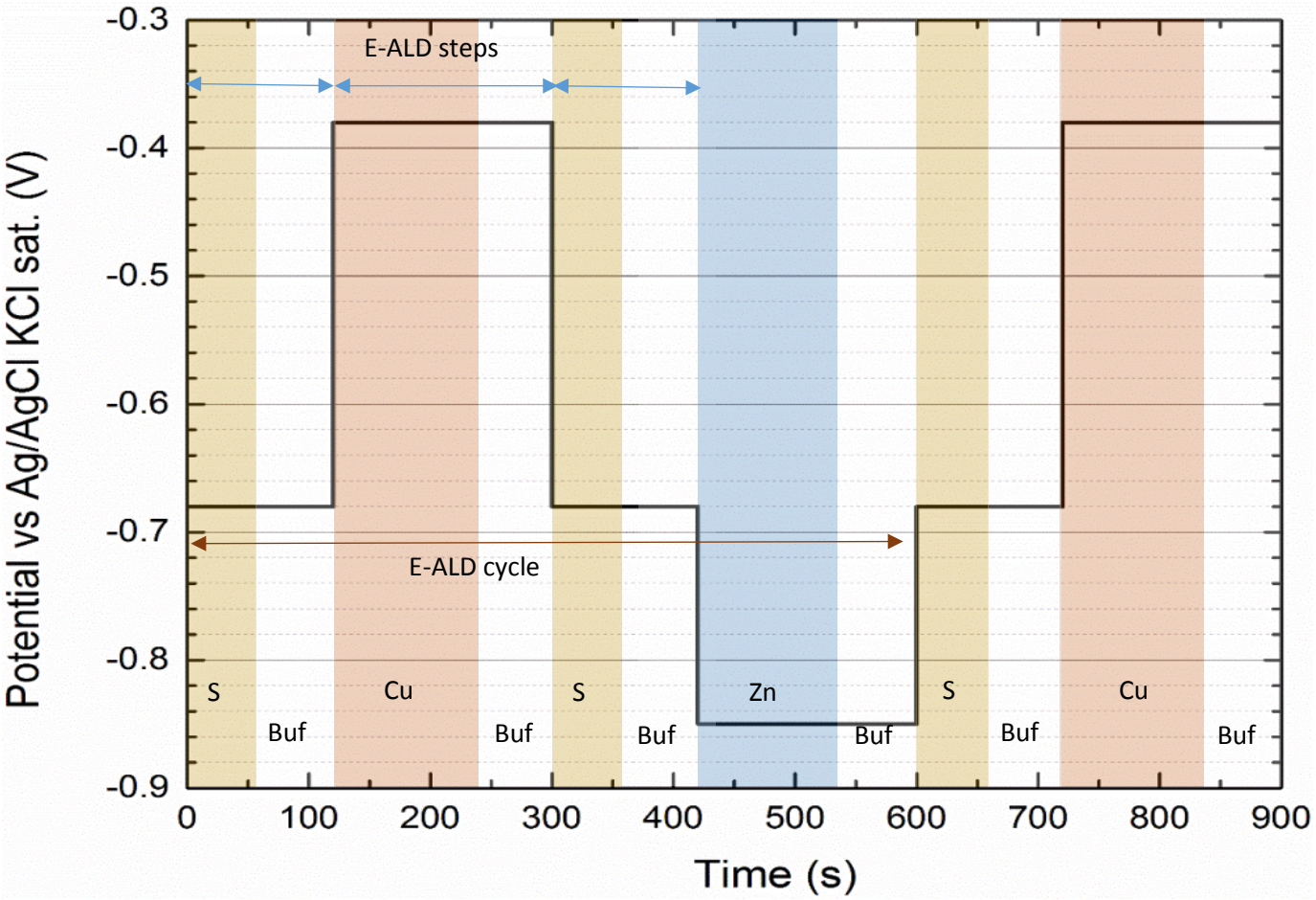

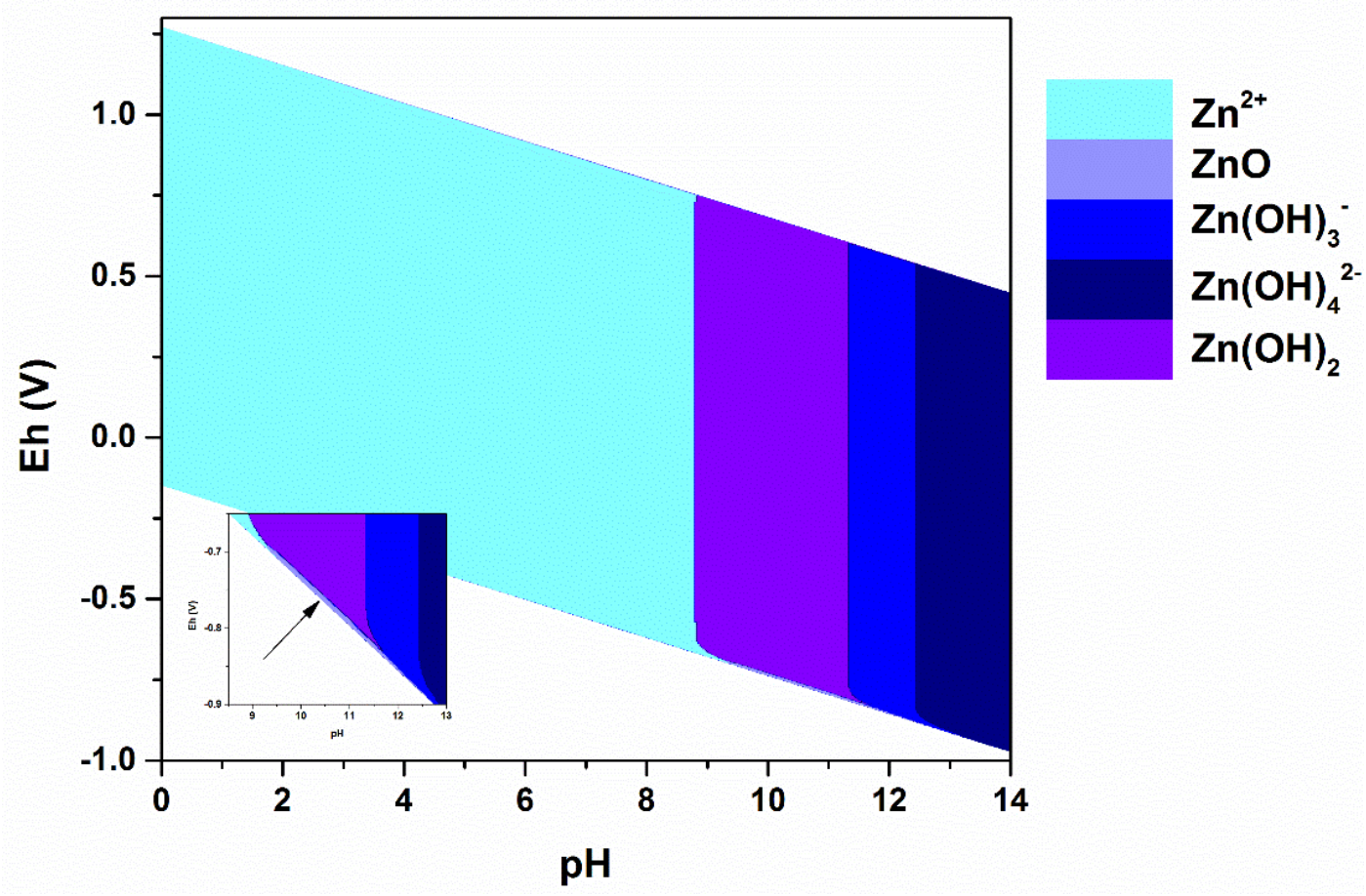

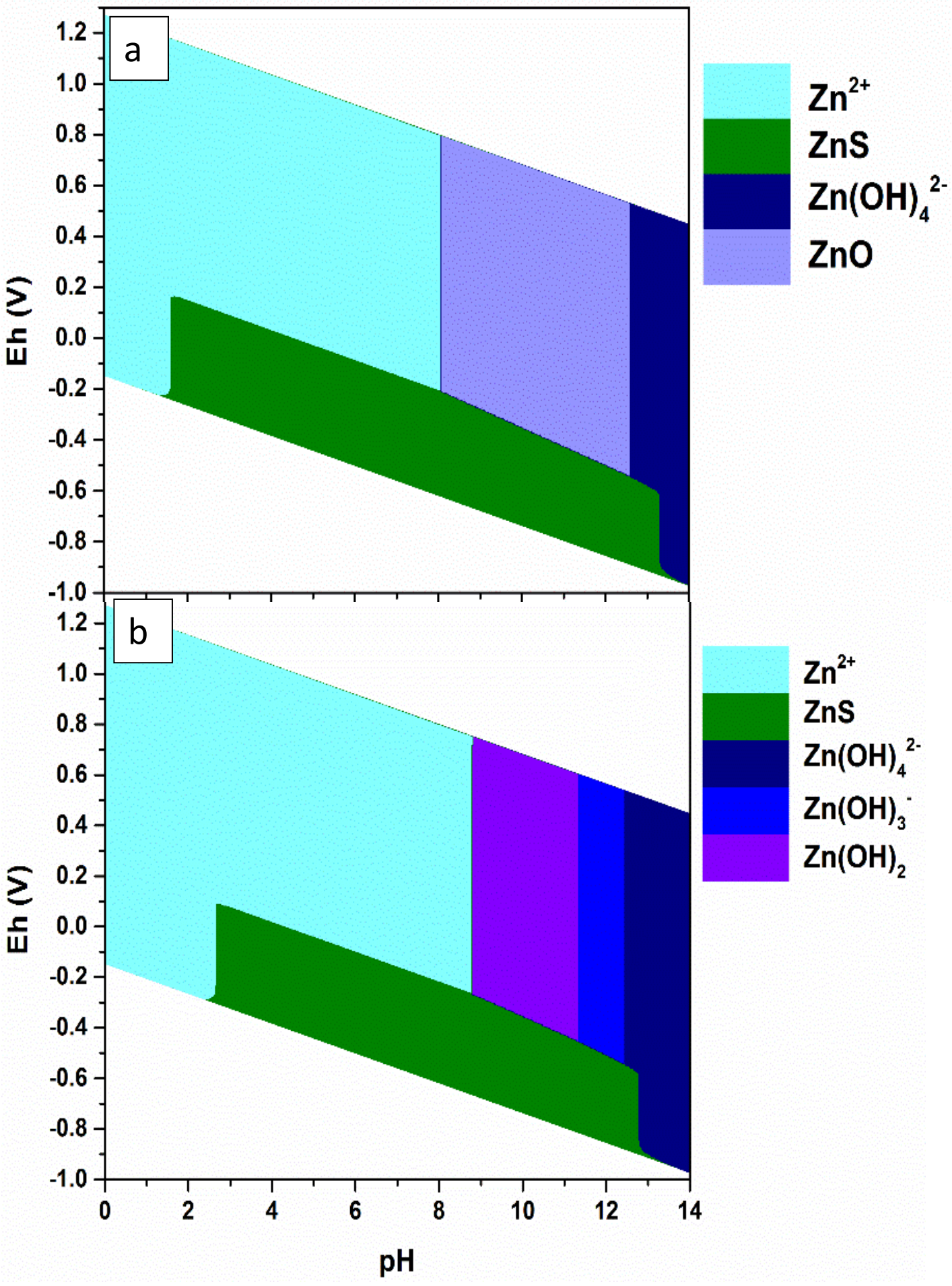
a
b
Eh (V)
pH
1.2
1.0
0.8
0.6
0.4
0.2
0.0
-0.2
-0.4
-0.6
-0.8
-1.0
0
2
4
6
8
10
12
14
Zn2+
ZnS
Zn(OH)4 2-
ZnO
Zn2+
ZnS
Zn(OH)4 2-
Zn(OH)3 -
Zn(OH)2

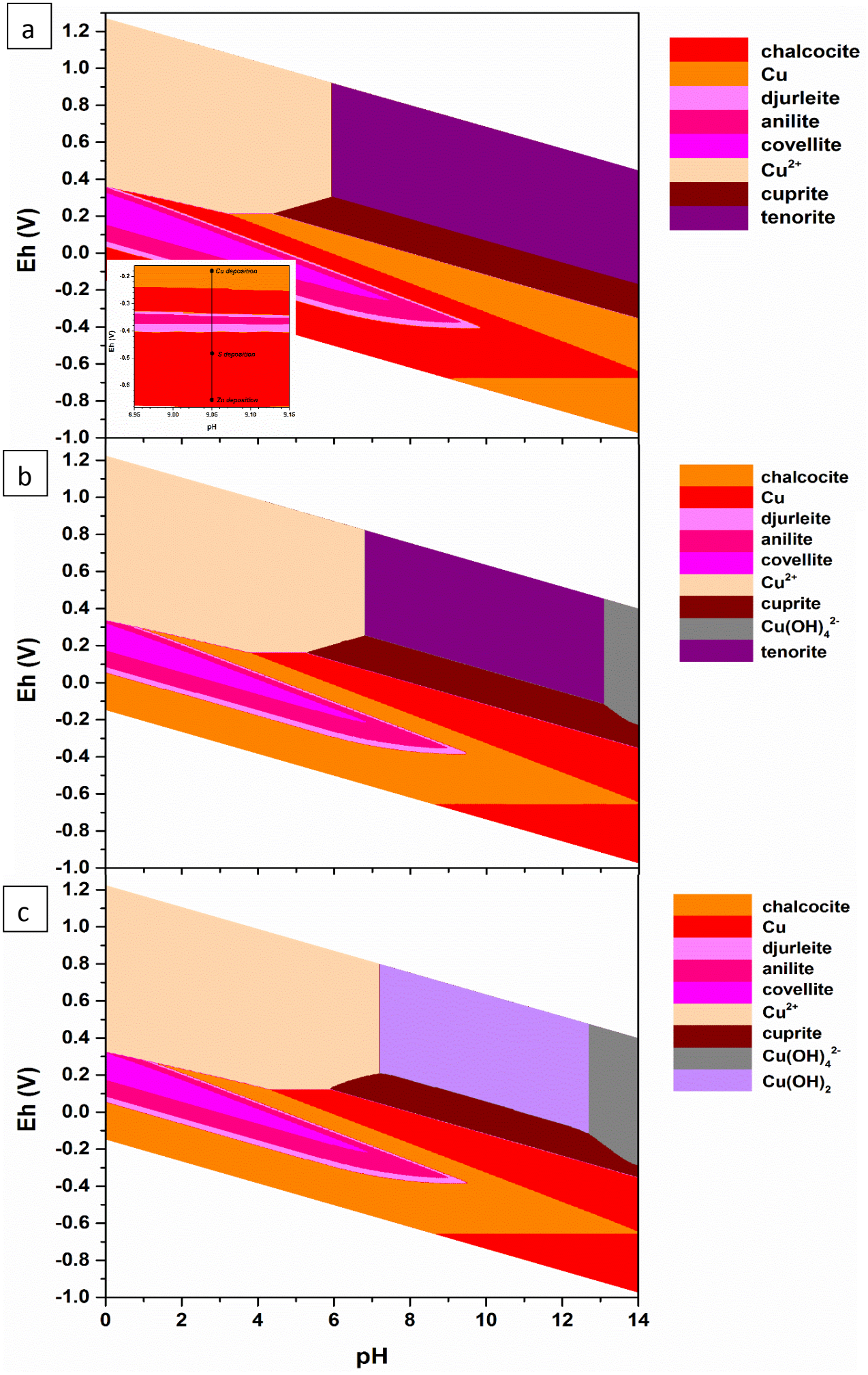
a
b
c
Eh (V)
pH
chalcocite
Cu
djurleite
anilite
covellite
Cu2+
cuprite
tenorite
Cu(OH)4 2-
Cu(OH)2
Cu deposition
S deposition
Zn deposition

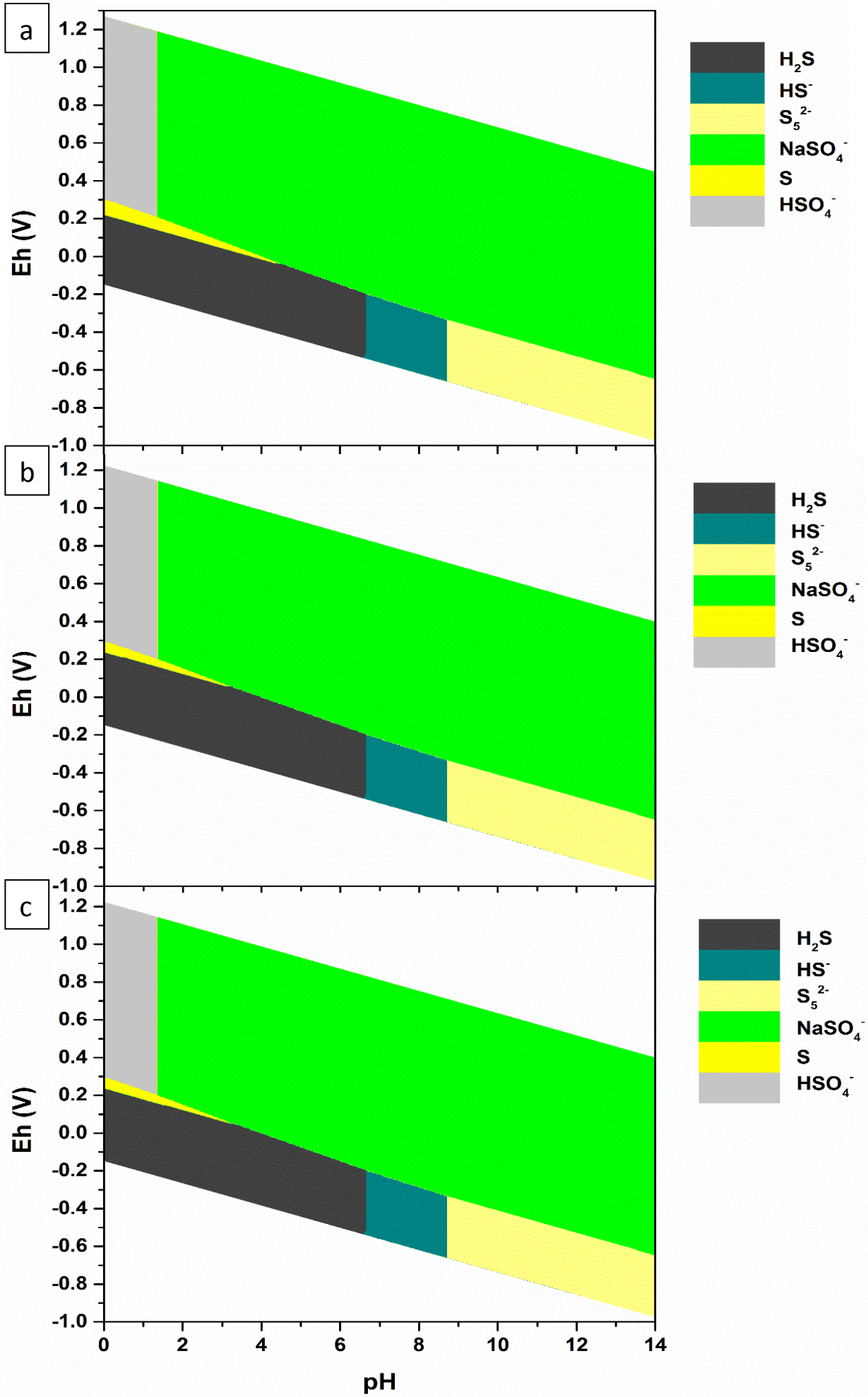
a
b
c
Eh (V)
pH
1.2
1.0
0.8
0.6
0.4
0.2
0.0
-0.2
-0.4
-0.6
-0.8
-1.0
0
2
4
6
8
10
12
14
H2S
HS-
S5 2-
NaSO4-
S
HSO4-

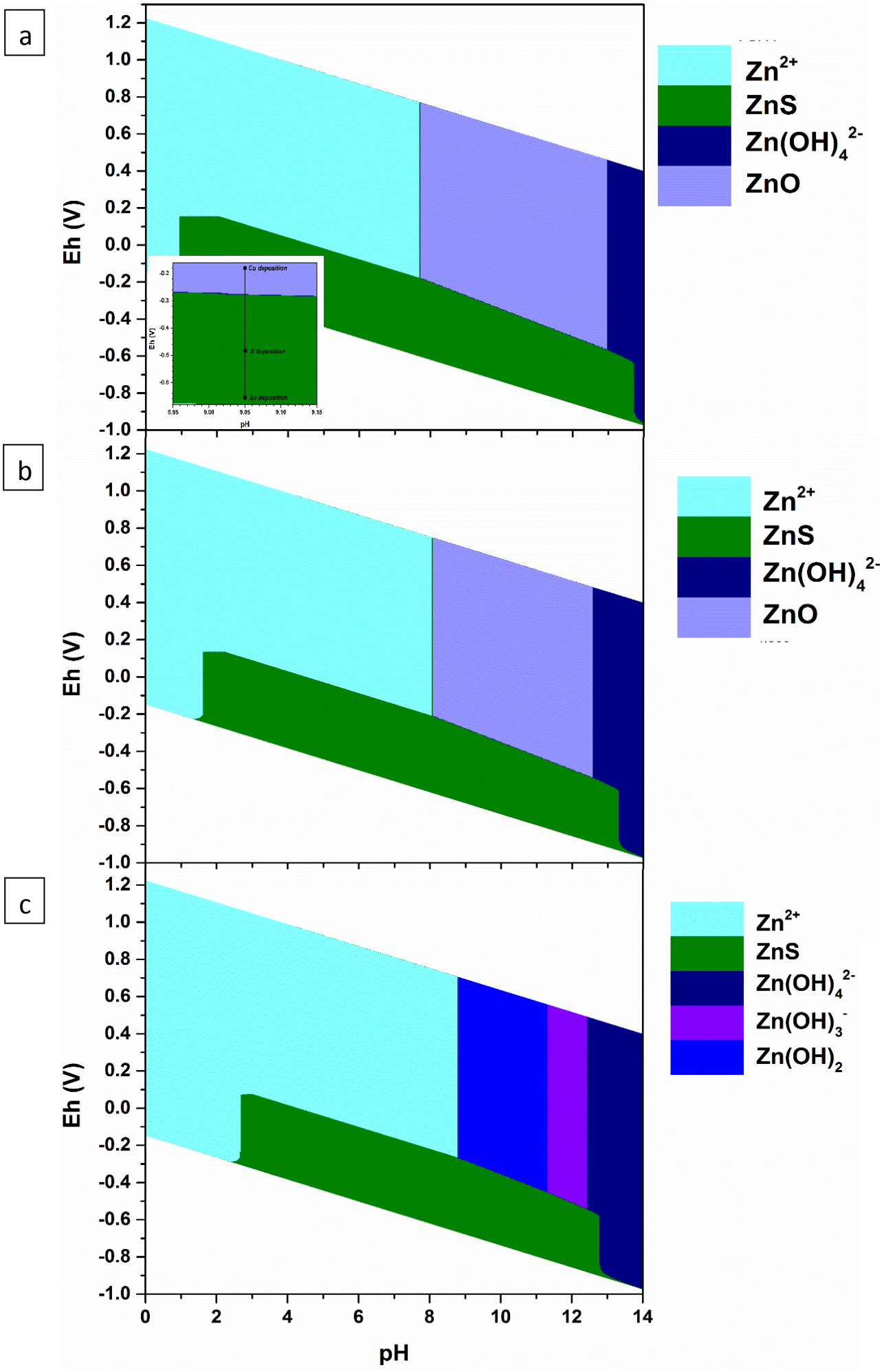
a
b
c
Eh (V)
pH
Zn2+
ZnS
Zn(OH)4 2-
ZnO
Zn(OH)3 -
Zn(OH)2
Cu deposition
S deposition
Zn deposition

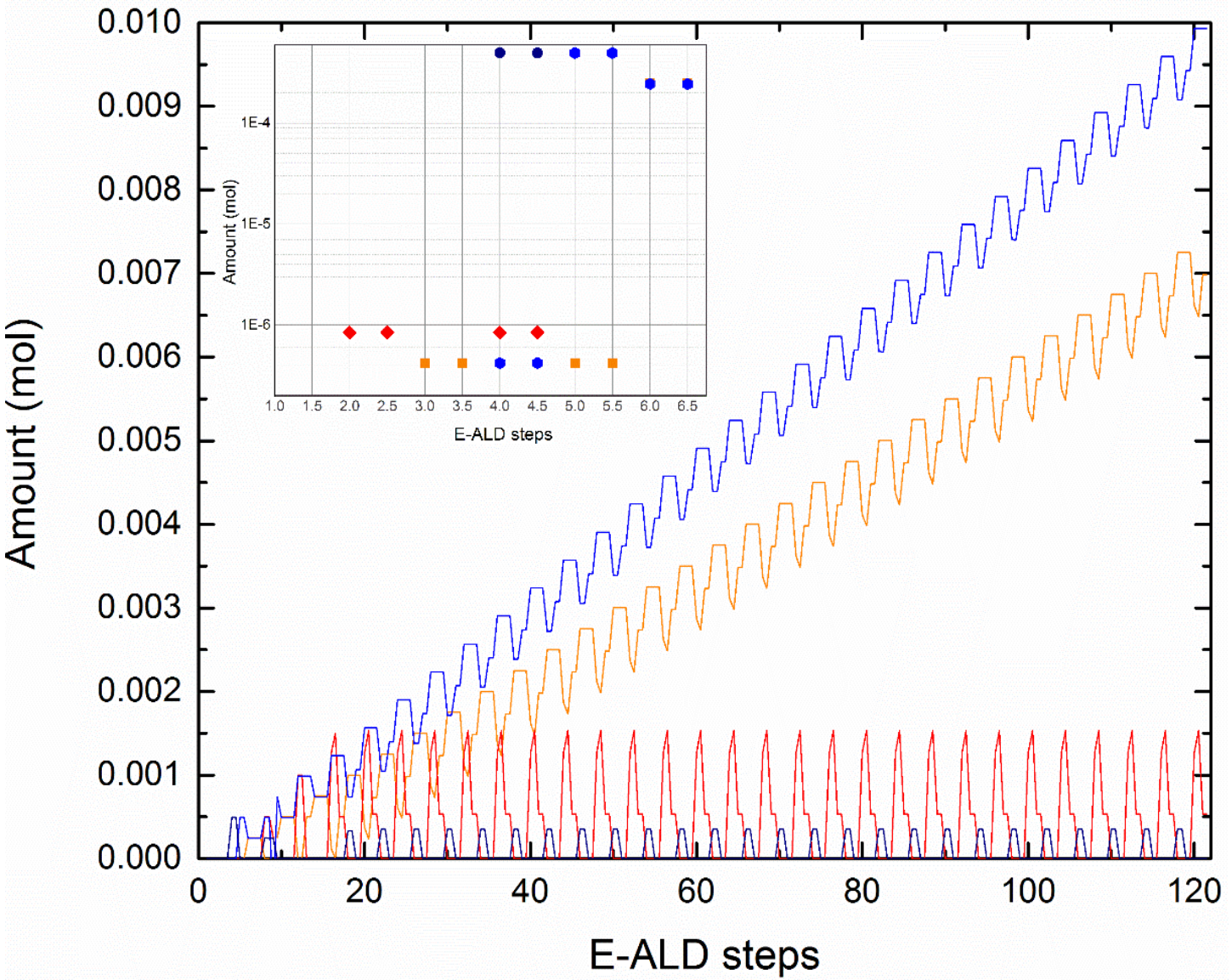
Amount (mol)
0.010
0.009
0.008
0.007
0.006
0.005
0.004
0.003
0.002
0.001
0.000
0
20
40
60
80
100
120
E-ALD steps
Amount (mol)
1E-4
1E-5
1E-6
1.0
1.5
2.0
2.5
3.0
3.5
4.0
4.5
5.0
5.5
6.0
6.5
E-ALD steps

a

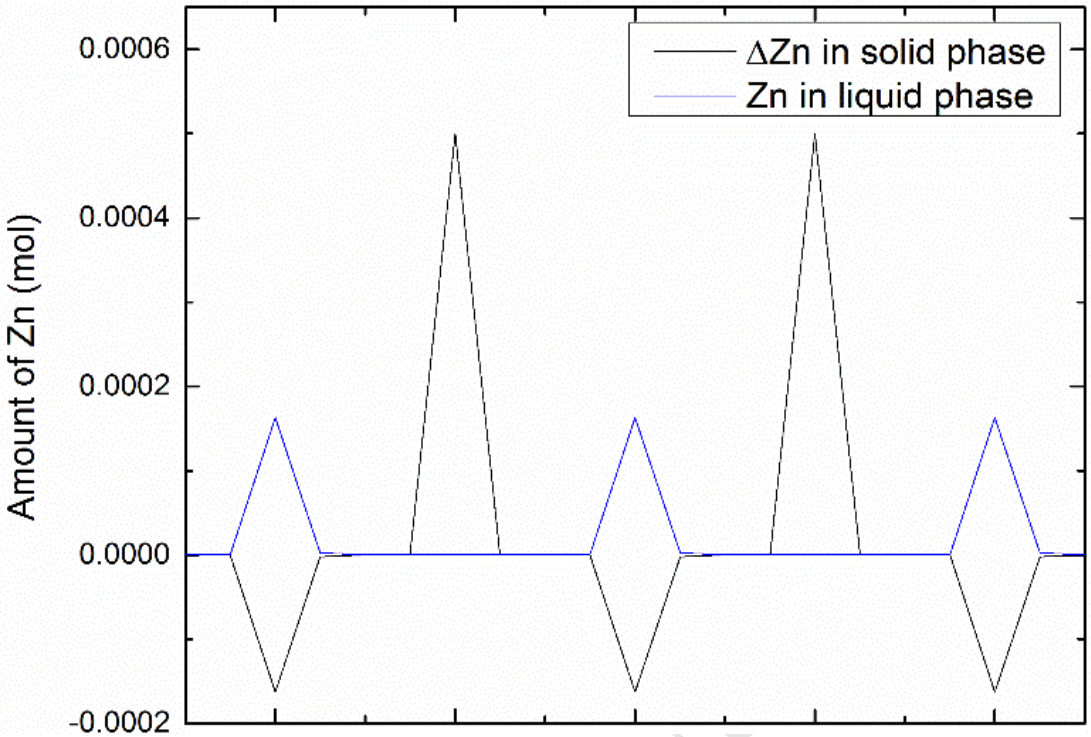
ΔZn in solid phase
Zn in liquid phase
Amount of Zn (mol)
0.0006
0.0004
0.0002
0.0000
-0.0002

b

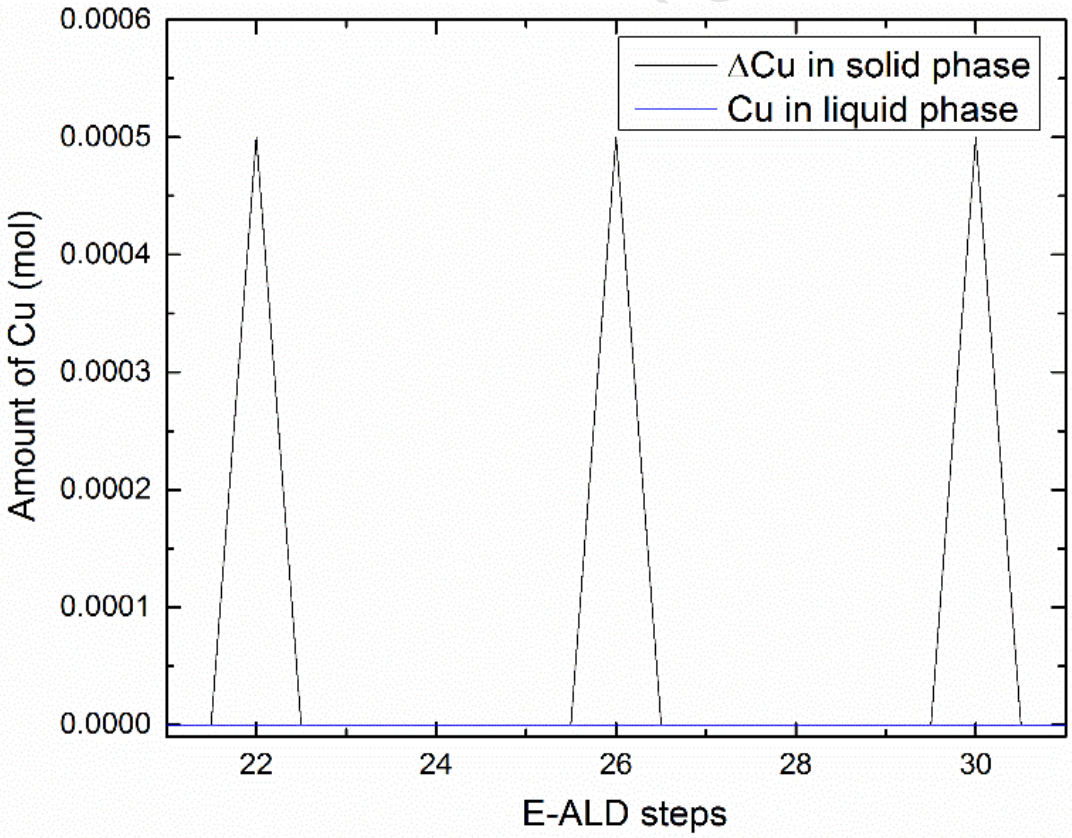
ΔCu in solid phase
Cu in liquid phase
Amount of Cu (mol)
0.0006
0.0005
0.0004
0.0003
0.0002
0.0001
0.0000
22
24
26
28
30
E-ALD steps

Highlights

- Phreeqc framework match the known Pourbaix diagrams involving Cu-S and Zn-S
- The main solid species involved in the E-ALD process are Chalcocite, Cu, Zincite and Sphalerite
- Two approximations result one in lower and higher boundaries for the Cu/Zn ratio
- During copper deposition Sphalerite is partially converted to Zincite and partially hydrolyzed
- Dissolution/precipitation reaction are compatible with the E-ALD process
- They could lead to the growth of the thread-like structure overgrowing the epitaxial phase